JOURNAL OF THE KOREAN ASTRONOMICAL SOCIETY
37: 249 ~ 255, 2004

PARKER-JEANS INSTABILITY IN THE GALACTIC GASEOUS DISK. I. LINEAR STABILITY ANALYSIS AND TWO-DIMENSIONAL MHD SIMULATIONS

S. M. LEE[1], JONGSOO KIM[2], J. FRANCO[3], AND S. S. HONG[4]
[1]Supercomputing Center, Korea Institute of Science & Technology Information, Eun-dong, Yuseong-ku, Daejeon, 305-308, Korea
E-mail: smlee@kisti.re.kr
[2]Korea Astronomy Observatory, Whaam-dong, Yuseong-ku, Daejeon, 305-348, Korea
[3]Instituto de Astronomía, Universidad Nacional Autónomia de México, Apartado Postal 70-264, Cd. Universitaria, 04510 Mexixo DF, CP 04510, Mexico
[4]Astronomy Program, SEES, Seoul National University, Shinlim-dong, Kwanak-ku, Seoul 151-742, Korea
(Received September 27, 2004; Accepted November 20, 2004)

ABSTRACT

Here we present a linear stability analysis and an MHD 2D model for the Parker-Jeans instability in the Galactic gaseous disk. The magnetic field is assumed parallel to a Galactic spiral arm, and the gaseous disk is modelled as a multi-component, magnetized, and isothermal gas layer. The model employs the observed vertical stratifications for the gas density and the gravitational acceleration in the Solar neighborhood, and the self-gravity of the gas is also included. By solving Poisson's equation for the gas density stratification, we determine the vertical acceleration due to self-gravity as a function of z. Subtracting it from the observed gravitational acceleration, we separate the total acceleration into self and external gravities. The linear stability analysis provides the corresponding dispersion relations. The time and length scales of the fastest growing mode of the Parker-Jeans instability are about 40 Myr and 3.3 kpc, respectively. In order to confirm the linear stability analysis, we have performed two-dimensional MHD simulations. These show that the Parker-Jeans instability under the self and external gravities evolves into a quasi-equilibrium state, creating condensations on the northern and southern sides of the plane, in an alternate manner.

Key words : Instabilities — ISM: HI superclouds — ISM: magnetic fields

I. INTRODUCTION

The general interstellar medium (ISM) of our Galaxy is composed of several diffuse and molecular gas components, and contains a large scale magnetic field that is, on average, parallel to the Galactic gaseous disk and provides partial support against the local gravitational field (e.g., Boulars & Cox 1990; Martos & Cox 1998; Martos et al. 1999). The stability of this gaseous disk has been studied, beginning with the pioneering work of Parker (1966), for several decades. In recent years, considering a multi-component model for the gaseous disk, Kim et al. (2000, hereafter Paper I) and Santillan et al. (2000, hereafter Paper II) performed two-dimensional linear stability analyses and nonlinear simulations of the evolution of the resulting Parker instabilities. They found that the time and length scales are larger than those of a thin model. Franco et al. (2002, hereafter Paper III) included the effects of spiral arms, and found that the instability creates a midplane-crossing distribution of massive condensations along the arm. These results could be associated with the corrugations, or wavy patterns, that are apparent in several gas and stellar tracers of the disk structure (Gum et al. 1960; Liszt 1985; Alfaro et al. 1992).

The models considered, however, that the local gravity is only due to the stars in the disk and halo (Bienayme et al. 1987), and did not include the role played by gravitational instabilities, which are capable of producing dense clouds (Elmegreen 1992, 1993). One obvious criticism to the above mentioned results, then, is that the Parker instability by itself is unable to produce the dense stages required to form molecular clouds (Kim & Hong 1998).

More recently, Lee (2002) and Lee & Hong (2004) have analyzed the evolution of the Parker-Jeans instability in self-gravitating disks. The Jeans mode can form clouds with high densities, and also tends to diminish the disruptive effects of the interchange mode (Lee & Hong 1999). Using a linear stability analysis for a multi-component disk under the effects of both (external and self-induced) gravities, here we show that the preferred mode of the combined instability leads to the formation of cloud condensations located alternatively up and down with respect to the midplane. The results of the linear analysis are verified with detailed two-dimensional simulations and, in forthcoming paper, we will later discuss the formation mechanism

Proceedings of The 2nd Korea-Mexico Joint Workshop on *Physics of the Diffuse Interstellar Medium*

of HI filamentary structures and GMCs that could be generated by the interchange and Jeans modes, respectively.

This paper is organized as follows: In § 2 we construct an initial equilibrium model for the gaseous disk, and § 3 describes the linear stability analysis. In § 4 we verify the results of the linear analysis with two-dimensional MHD simulations. Finally, a brief summary and discussions are given in § 5. Some details of the linearized equations are given in the Appendix.

II. MHD MODEL FOR THE GALACTIC GASEOUS DISK

Our initial Galactic disk model is the one described by Boulares & Cox (1990). The model considers five interstellar gas layers, and we further assume that all of them are isothermal and with the same temperature. Here we also consider, in a separate form, the gravitational accelerations generated by the stellar component and by the ISM itself. That is, an externally given Galactic gravity, $\boldsymbol{g}_{\rm ext}$, and the self-gravity of the gaseous disk, $\boldsymbol{g}_{\rm self}$. The external gravity remains fixed in time and is perpendicular to the disk. It has only a vertical component, namely, $\boldsymbol{g}_{\rm ext}$= [0, 0, $-g_{\rm ext}$], with $g_{\rm ext} \geq 0$. The self-gravitational acceleration, on the other hand, varies in time and can have components in all 3 coordinates. The initial self-gravity, however, has only a vertical component, $\boldsymbol{g}_{\rm self,o}$= [0, 0, $-g_{\rm self,o}$], with $g_{\rm self,o} \geq 0$. For this we use the gravitational acceleration at the Solar Neighborhood derived by Bienaymé et al. (1987), and assume that it is equal to the sum of $g_{\rm ext}$ and $g_{\rm self,o}$. In addition, we derive $g_{\rm self,o}$ as a function of Galactic latitude, z, by solving Poisson's equation with the density stratification from Boulares & Cox (1990).

The assumed ISM density is then,

$$\begin{aligned} \mathrm{n_o}(z) = 0.6 \exp\left[-\frac{z^2}{2(70\mathrm{pc})^2}\right] \\ +0.3 \exp\left[-\frac{z^2}{2(135\mathrm{pc})^2}\right] \\ +0.07 \exp\left[-\frac{z^2}{2(135\mathrm{pc})^2}\right] \\ +0.1 \exp\left[-\frac{|z|}{400\mathrm{pc}}\right] \\ +0.03 \exp\left[-\frac{|z|}{900\mathrm{pc}}\right], \end{aligned} \quad (1)$$

where each gas component represents the contributions of H_2, cold HI, warm HI in clouds, warm intercloud HI, and warm diffuse HII, respectively.

The gravitational acceleration from Bienaymé et al. (1987) is fitted with the approximation given by Martos (1993) as follow:

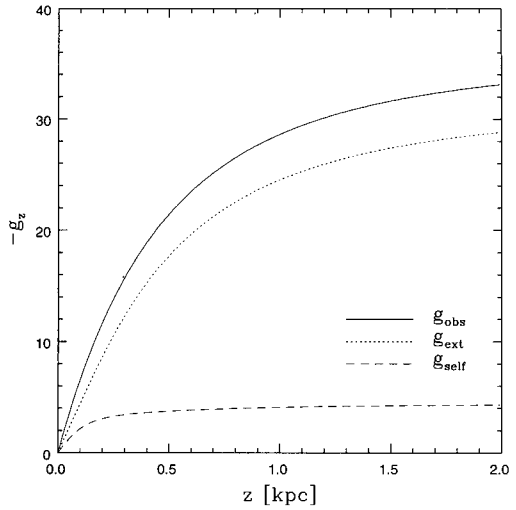

Fig. 1.— Galactic gravitational acceleration. Solid line means observed gravity, dotted line represents gravity from stars, and dashed line is the self-gravitational acceleration from all gaseous components. Self-gravity represents about 13 percent of the observed total gravity. The ordinate denotes the normalized Galactic vertical gravitational acceleration in units of Lc_s^2.

$$g_{\rm obs}(z) = 8 \times 10^{-9} \left[1 - 0.52 \exp\left(-\frac{|z|}{325\mathrm{pc}}\right) - 0.48 \exp\left(-\frac{|z|}{900\mathrm{pc}}\right)\right] \mathrm{cm\,s^{-2}}. \quad (2)$$

The initial equilibrium configuration is generated by assuming that the gas is isothermal, and the initial magnetic field is aligned along a spiral arm, varying with the vertical distance, z, from midplane, i.e., $\mathbf{B_o}$=[0, $\mathrm{B_o}(z)$, 0]. The vertical structure of the initial equilibrium disk is then described by:

$$\frac{\mathrm{d}}{\mathrm{dz}}\mathrm{P_o}(z) = \frac{\mathrm{d}}{\mathrm{dz}}\left[\rho_{\rm o}(z)\mathrm{c_s^2} + \frac{\mathrm{B_o^2}(z)}{8\pi}\right] = -\rho_{\rm o}(z)\mathrm{g_{obs}}(z), \quad (3)$$

where $\mathrm{P_o}(z)$ is the total pressure of the system (gaseous and magnetic), and $\rho_{\rm o}(z) = 1.27\, m_{\rm H} n_{\rm o}(z)$ is the density (the midplane value is $n_{\rm o}(0) \simeq 1.1$ cm^{-3}, including 10% of He by number). Given the total pressure ($\mathrm{P_o}(0) \sim 3 \times 10^{-12}$ dyn cm^{-2}, Boulares & Cox 1990) and magnetic strength ($\mathrm{B_o}(0) \simeq 5\mu$G, Heiles 1995) at the midplane, the resulting isothermal sound speed is c_s=8.4 km s^{-1}. With these values for the density stratification, gravitational field, and sound speed, we obtain the stratification of the B-field by solving Eq. (3). The details are described in Paper I.

The strength of $g_{\rm self,o}$ amounts to only about 13% of the total gravitational acceleration, $g_{\rm obs}$, and we define the external component as $g_{\rm ext} = g_{\rm obs} - g_{\rm self,o}$. For simplicity, as indicated before, we further assume that this

external component is time independent and directed along the z-axis. In contrast, the self-gravitational component varies as some gas condensations are formed, generating forces along all three coordinate axes. This difference already indicates that the inclusion of self-gravity will have different consequences to those discussed in Papers I, II, and III.

III. LINEAR STABILITY ANALYSIS

(a) Ideal Magnetohydrodynamical Equations

The dynamics of a magnetized plasma under the influences of self and external gravities is described by the ideal MHD equations

$$\frac{\partial \rho}{\partial t} + \nabla \cdot (\rho \boldsymbol{v}) = 0, \tag{4}$$

$$\rho \left(\frac{\partial \mathbf{v}}{\partial t} + \boldsymbol{v} \cdot \nabla \boldsymbol{v} \right) = -\nabla P + \frac{1}{4\pi} (\nabla \times \boldsymbol{B}) \times \boldsymbol{B} - \rho \nabla \psi_{\rm s} + \rho \boldsymbol{g}_{\rm ext}, \tag{5}$$

$$\frac{\partial \boldsymbol{B}}{\partial t} = \nabla \times (\boldsymbol{v} \times \boldsymbol{B}), \tag{6}$$

$$\nabla^2 \psi_{\rm s} = 4\pi G \rho, \tag{7}$$

$$\frac{d}{dt} (P/\rho^{\gamma}) = 0, \tag{8}$$

where $\psi_{\rm s}$ is the self gravitational potential, and the rest of the symbols have their usual meanings. We use a Cartesian coordinate system (x, y, z), whose axes are in the radial, azimuthal and vertical directions of the disk, respectively. The azimuthal direction is here identified with the direction of a local spiral arm.

(b) Linearization and Perturbation Equations

The linearized versions of the ideal MHD equations under the influences of self and external gravities are given by

$$\frac{\partial}{\partial t} \rho_1 + \nabla \cdot (\rho_{\rm o} \boldsymbol{v}) = 0, \tag{9}$$

$$\rho_{\rm o} \frac{\partial}{\partial t} \boldsymbol{v} = -\nabla P_1 + \frac{1}{4\pi} (\nabla \times \boldsymbol{B}_1) \times \mathbf{B}_{\rm o} + \frac{1}{4\pi} (\nabla \times \mathbf{B}_{\rm o}) \times \boldsymbol{B}_1 - \rho_{\rm o} \nabla \psi_{\rm s,1} + \rho_1 \boldsymbol{g}_{\rm self,o} + \rho_1 \boldsymbol{g}_{\rm ext}, \tag{10}$$

$$\frac{\partial}{\partial t} \boldsymbol{B}_1 = \nabla \times (\boldsymbol{v} \times \mathbf{B}_{\rm o}), \tag{11}$$

$$\nabla^2 \psi_{\rm s,1} = 4\pi G \rho_1. \tag{12}$$

$$\frac{\partial}{\partial t} P_1 + \gamma \mathrm{P_o} \nabla \cdot \boldsymbol{v} + (\boldsymbol{v} \cdot \nabla) \mathrm{P_o} = 0. \tag{13}$$

The symbols with subscript 1 denote the perturbed values. The gas disk extends to infinity in the x- and y-directions, and is bounded by the Galactic halo at $z = \pm z_h$. The position of the Galactic halo, z_h, corresponds to the maximum disk thickness, $z_{\rm max}$.

For the unperturbed material we take the isothermal equation of state, $P = \rho c_s^2$, while for the perturbed gas we use the barotropic relation $P = \kappa \rho^{\gamma}$. As stated before, all gas layers are assumed isothermal, with a sound speed of 8.4 km s^{-1}, and number density at mid-plane of 1.1 cm^{-3}. The effective scale height of our multi-component disk is about 166 pc (see, Paper I) but the resulting structures are much larger and, for convenience, we fix the length scale, L, at 1 kpc. Then, the time unit is about 120 Myr. Since the initial magnetic and gas pressures do not vary in the same fashion with vertical distance, we follow the ratio, $\alpha(z) = \mathrm{B_o^2}(z)/8\pi \mathrm{P_o}(z)$, as a function of z.

Seeking solutions of the form

$$q_1(x, y, z, t) = q_1(z) \ \exp\left[i(k_x x + k_y y - \omega t)\right], \tag{14}$$

and adopting L and c_s as units of length and velocity, we recast the set of linearized equations as

$$\Omega \frac{n_1}{\mathrm{n_o}} = i\xi u_x + i\eta u_y + \frac{d}{d\zeta} u_z - \Theta_n u_z, \tag{15}$$

$$\Omega u_x = i\xi \frac{P_1}{\mathrm{P_o}} - 2i\eta\alpha \frac{B_{1x}}{\mathrm{B_o}} + 2i\xi\alpha \frac{B_{1y}}{\mathrm{B_o}} + i\xi\phi, \tag{16}$$

$$\Omega u_y = i\eta \frac{P_1}{\mathrm{P_o}} + 2\alpha\Theta_b + i\eta\phi, \tag{17}$$

$$\Omega u_z = \frac{d}{d\zeta} \frac{P_1}{\mathrm{P_o}} - \Theta_n \frac{P_1}{\mathrm{P_o}} - 2i\eta\alpha \frac{B_{1z}}{\mathrm{B_o}} - 4\alpha\Theta_b \frac{B_{1y}}{\mathrm{B_o}} + 2\alpha \frac{d}{d\zeta} \frac{B_{1y}}{B_o} + \frac{d}{d\zeta}\phi + \left[(1+\alpha)\Theta_n - \frac{d}{d\zeta}\alpha \right] \frac{n_1}{\mathrm{n_o}}, \tag{18}$$

$$\Omega \frac{B_{1x}}{\mathrm{B_o}} = -i\eta u_x, \tag{19}$$

$$\Omega \frac{B_{1y}}{\mathrm{B_o}} = \frac{d}{d\zeta} u_z - \Theta_b u_z + i\xi u_x, \tag{20}$$

$$\Omega \frac{B_{1z}}{\mathrm{B_o}} = -i\eta u_z, \tag{21}$$

$$\Omega \frac{P_1}{\mathrm{P_o}} = -\Theta_n u_z + \gamma \left(i\xi u_x + i\eta u_y + \frac{d}{d\zeta} u_z \right), \tag{22}$$

$$\frac{d^2}{d\zeta^2}\phi - (\xi^2 + \eta^2)\phi = S_v \frac{n_1}{\mathrm{n_o}}. \tag{23}$$

Here, $u_x = v_x/c_s$, $u_y = v_y/c_s$, $u_z = v_z/c_s$, $\phi = \psi_{\rm s,1}/c_s^2$, $\xi = k_x L$, $\eta = k_y L$, $\zeta = z/L$, and $\Omega = \omega L/\mathrm{c_s}$ are all dimensionless quantities, and for simplicity, we define $\Theta_n = -d \ln \mathrm{n_o}/d\zeta$, $\Theta_b = -d \ln \mathrm{B_o}/d\zeta$, and $S_v(\zeta) = 4\pi \mathrm{G} L^2 \mu \mathrm{m_H} \mathrm{n_o}(\zeta)/\mathrm{c_s^2}$, where $\mu = 1.27$ is the mean molecular weight of the multi-component gas disk.

Eliminating all the variables in favor of u_z and ϕ, we combine equations (15) through (23) into the following two second-order ordinary differential equations:

$$A_2 \frac{d^2}{d\zeta^2} u_z + A_1 \frac{d}{d\zeta} u_z + A_0 u_z = B_1 \frac{d}{d\zeta}\phi + B_0 \phi \tag{24}$$

and

$$C_2\frac{d^2}{d\zeta^2}\phi + C_0\phi = D_1\frac{d}{d\zeta}u_z + D_0 u_z. \qquad (25)$$

The coefficients, A_0, A_1, A_2, B_0, B_1, C_0, C_2, D_0, and D_1 are described in the Appendix.

In order to fix the boundary conditions at $\zeta = \pm\zeta_h$, we follow Tomisaka & Ikeuchi (1983). The vertical component of the perturbed velocity at the boundary should satisfy $-i\Omega\delta\zeta = u_z(\zeta_h)$.

Applying Gauss flux theorem to the perturbed boundary gives

$$-\sqrt{\xi^2+\eta^2}\phi(\zeta_h) - \left.\frac{d}{d\zeta}\phi\right|_{\zeta_h} = S_v(\zeta_h)\delta\zeta. \qquad (26)$$

The third boundary condition is found from pressure continuity; the sum of gas and magnetic pressures should be kept continuous at the boundary. By integrating the z-component of the MHD momentum equation from z_h to $z_h+\delta z$, one may obtain the boundary condition as

$$\frac{\gamma\Omega W}{S_v(\zeta_a)}\left[\frac{d^2}{d\zeta^2}\phi - k^2\phi\right] + \left\{(\gamma-1)\Theta_n + \frac{2\alpha\eta^2}{k}\right\} W u_z$$

$$-2\alpha\left[\Theta_b\Omega^4 + \left\{(\gamma\Theta_b - \Theta_n)\xi^2 + (2\alpha+\gamma)\Theta_n\eta^2\right\}\Omega^2\right] u_z$$

$$+W\Omega g_{\rm obs}(\zeta_a)\delta\zeta + 2\alpha(\Omega^2+2\alpha\eta^2)(\Omega^2+\gamma\eta^2)\frac{d}{d\zeta}u_z$$

$$-2\alpha\xi^2\Omega^3\phi - 4\alpha^2\gamma\Theta_b\eta^2k^2u_z = 0, \qquad (27)$$

where k means $\sqrt{\xi^2+\eta^2}$, and W does $\Omega^4 + (2\alpha+\gamma)k^2\Omega^2 + 2\alpha\gamma\eta^2k^2$.

In addition to these conditions, the mode parity should be specified at mid-plane. If symmetric (odd-parity) perturbations are chosen for the vertical velocity, the solution should satisfy

$$\left.\frac{d}{d\zeta}\phi\right|_{\zeta=0} = 0 \text{ and } u_z(\zeta=0) = 0. \qquad (28)$$

These odd-parity perturbations result in solutions with reflection symmetry about the midplane. For anti-symmetric (even-parity) perturbations, the solution should satisfy

$$\phi(\zeta=0) = 0 \text{ and } \left.\frac{d}{d\zeta}u_z\right|_{\zeta=0} = 0. \qquad (29)$$

These even-parity solutions, in turn, result in midplane crossing structures.

In this paper, we limit the discussion to perturbations in the (y, z)-plane. With this limitation we can only follow the undular branch of the instability, and the models are performed in the isothermal mode, with $\gamma = 1$. The dispersion relations are obtained with the method described in Lee (2002), and the eigenvector components are initially fixed by the upper boundary conditions. For a given perturbation wave number, we take a trial value and then integrate the equations with the fourth-order *Runge-Kutta* method. When the resulting solution satisfies the chosen parity condition at z=0, the trial solution is adopted as the eigenvalue.

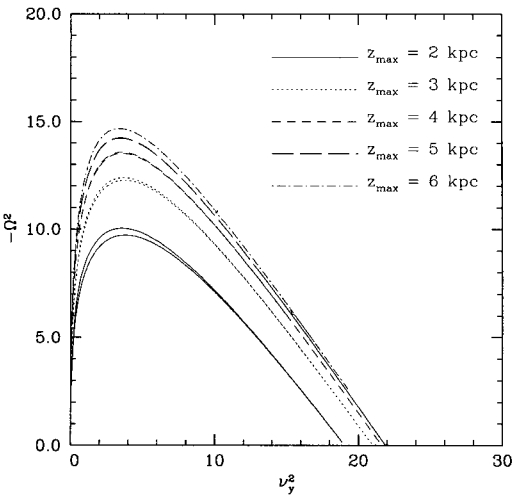

Fig. 2.— Dispersion relations for the undular mode in a magnetized multi-component gas disk. Each curve is marked by the value of the maximum disk thickness considered, $z_{\rm max}$. The ordinate corresponds to the square of the normalized growth rate, and the abscissa to the square of the normalized y-directional wave number. The normalization units are the isothermal sound speed, c_s=8.4 km s^{-1}, and length scale, L=1 kpc.

(c) Dispersion Relations

The resulting dispersion relations are shown in Figure 2 for five cases with upper boundaries between 2 and 6 kpc. For the lowest boundary surface, $z_{\rm max}$=2 kpc, the fastest growing time is about 3.9×10^7 yr, and its wavelength is 3.32 kpc. For the highest boundary surface, $z_{\rm max}$ = 6 kpc, the corresponding values change to 3.1×10^7 yr and 3.39 kpc, respectively. Comparing with the results of Paper I, the growth time decreases by about 15%, and the corresponding length scale increases about 10% (see Table I). This is due to the inclusion of self-gravity, which helps the combined instability to grow slightly faster than the pure undular instability does. For each case, we have calculated the dispersion curves for both midplane-symmetric and midplane-crossing perturbations. In two-dimensions, the growth rates of both modes in the combined Parker-Jeans instability are larger than those of the pure Parker instability. The midplane-crossing perturbations generate condensations at the upper and lower hemispheres in an alternate fashion, and grow faster than the midplane-symmetric perturbations. This is in contrast with the pure gravitational instability, that

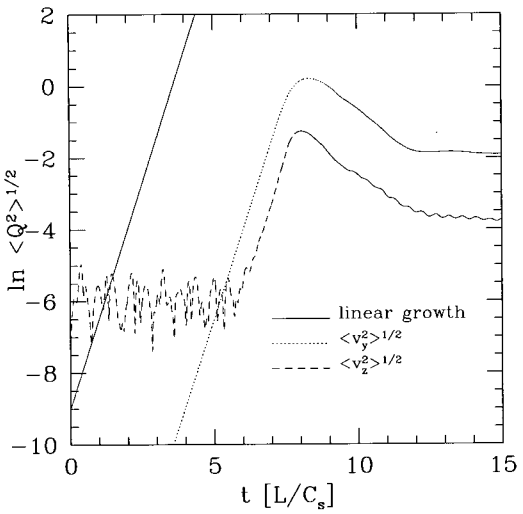

Fig. 3.— Run of the *rms* velocities as a function of time. The natural log is used along the ordinate. The solid line has a slope equal to the growth rate for the fastest growing undular mode. After about $t = 10$, the gas disk enter into the relaxation state, and eventually evolves into a dynamical quasi-equilibrium state.

prefers the midplane symmetric mode. The preferred parity of the combined the Parker-Jeans instability results in midplane-crossing features, just like the corrugations observed in spiral arms. Thus, the instability in our case follows the one of the pure Parker instability because self-gravity amounts to only 13% of the total gravity.

IV. TWO-DIMENSIONAL SIMULATIONS

The wavelength and parity of the fastest growing mode in our multi-component gas disk is verified with the aid of two-dimensional MHD simulations. The models, that use random velocity perturbations to trigger the instability, are performed with the isothermal MHD TVD code written by Kim et al. (1999) and a Poisson solver that uses the FFT method along with the Green function (Lee 2002). Here we show the dynamical evolution for the 2 kpc half thickness case using a grid with 256^2 zones. The physical sizes for this computational domain are 16×4 kpc^2, with a linear resolution ranging from 15 to 63 pc. The initial state is in equilibrium and receives random velocity perturbations with an amplitude of 10^{-4} c_s. Galactic differential rotation is not included.

Figure 3 shows the *rms* values for the resulting azimuthal (dotted line) and vertical (dashed line) velocities as a function of time. The solid line has a slope equal to the growth rate for the fastest growing mode with $z_{\rm max}$ =2 kpc derived from the linear stability analysis. As is clear from the figure, the growth rate of the linear part in the simulation follows the predicted rate for this case.

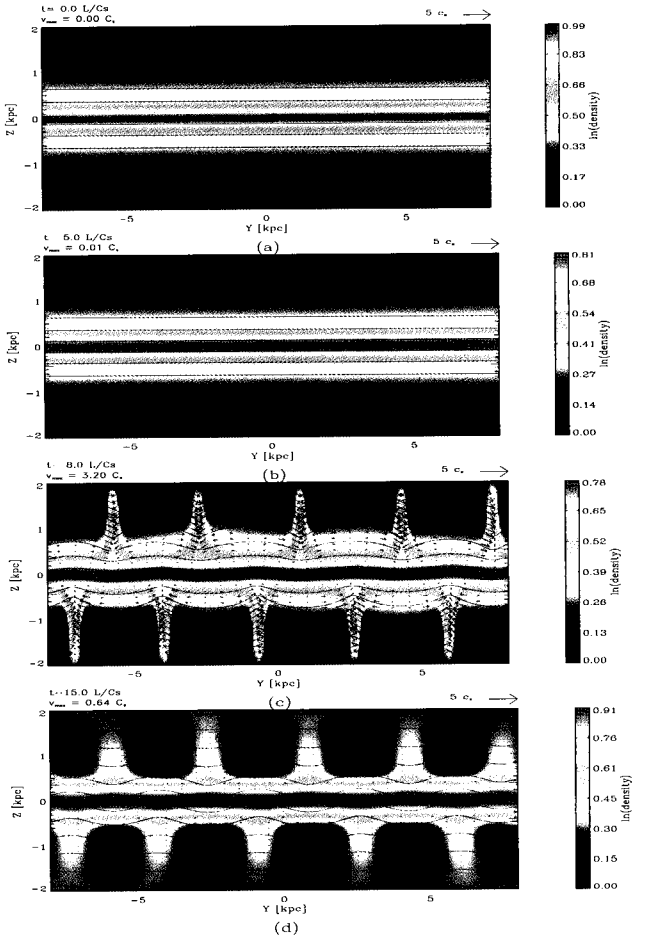

Fig. 4.— Time-series maps of the Parker-Jeans instability in 2D. The sequence shows the density (rainbow logarithmic scale), velocity field (arrows), and magnetic field (lines), at four selected times: t=0.0, 5.0, 8.0, and 15.0 L/c_s. a) Initial stage, b) vertical oscillation stage, c) linearly growing stage, and d) quasi-equilibrium state.

Figures 4 shows snapshots of the resulting density structures at four selected times with t=0, 5, 8 and 10. As predicted by the linear stability analysis, the condensations in the magnetic valleys are distributed in a corrugation-like fashion, and the separations are equal to the wavelength of the fastest growing mode. This shows that the midplane-crossing mode is effectively the dominant mode in this model.

Also, Figures 4c and 4d show that the velocity field in the magnetic valleys form zero-velocity regions. This implies that the evolution of the two-dimensional disk tends eventually to an equilibrium state similar to that found in the cases without self-gravity, as those discussed in Papers I and II. Again, this is because self-gravity only amounts to 13% of the total gravitational acceleration, and simply adds an additional force to drive the material faster into the magnetic valleys.

TABLE 1
MAXIMUM GROWTH RATES AND WAVELENGTHS FOR "EXTERNAL" AND "BOTH" GRAVITIES

z_{max}	$\Omega_{max,ext}$	$\tau_{min,ext}$ [years]	$\lambda_{y,max,ext}$ [kpc]	$\Omega_{max,both}$	$\tau_{min,both}$ [years]	$\lambda_{y,max,both}$ [kpc]
1.5	1.81	6.4×10^7	1.50	-	-	-
2.0	2.56	4.6×10^7	3.01	3.16	3.9×10^7	3.32
3.0	3.01	3.9×10^7	3.30	3.52	3.3×10^7	3.34
4.0	3.24	3.6×10^7	3.48	3.36	3.2×10^7	3.36
5.0	3.41	3.4×10^7	3.69	3.77	3.1×10^7	3.39

V. DISCUSSION AND SUMMARY

Here we have presented a model for the Parker-Jeans instability under the influence of self and external gravities in a thick gaseous disk. We have assumed a magnetized, isothermal, and multi-component gaseous disk that is unstable to the Parker instability. The initial magnetic field lines run parallel to the spiral arm. Under Galactic conditions for the gravitational acceleration, gas structure, and magnetic field strength, the resulting large-scale structures prefer to be distributed in an azimuthally corrugated pattern. For the case of a half disk thickness of 2 kpc, the wavelength of the fastest growing mode along the arm is about 3.3 kpc. The most relevant outcome of this study is the role played by the Parker-Jeans instability in forming large-scale and dense structures along spiral arms.

The principal results of the two-dimensional models are as follows: (1) The inclusion of self-gravity speeds up the growth time scale by about 15%, and the corresponding length scale increases by about 10%. (2) As the undular mode grows along the direction of the arm, the Parker instability generates gas condensations distributed in an alternate manner with respect to the midplane. This second result is in line with the results found in Paper III.

Elmegreen & Elmegreen (1987) described large HI condensations observed in external galaxies, which they called superclouds. They suggested that these objects form from the diffuse medium due to gravitational instabilities. Our model indicates that these HI superclouds can be generated by the undular mode of the Parker instability along spiral arms.

ACKNOWLEDGEMENTS

We warmly thank B.-C. Koo for useful comments and suggestions. This work has been partially supported by DGAPA-UNAM grant. The numerical calculations were performed using UNAM's ORIGIN-2000 supercomputer and IBM p690 at KISTI Supercomputing Center.

APPENDIX

COEFFICIENTS OF PERTURBATION EQUATIONS

In section 3, we derived two second order ordinary differential equations in terms of u_z and ϕ. The coefficients for equations (11) and (12) are:

$$A_2 \equiv (\Omega^2 + 2\alpha\eta^2)\left\{(2\alpha+\gamma)\Omega^2 + 2\alpha\gamma\eta^2\right\}$$

$$A_1 \equiv 2\frac{d\alpha}{d\zeta}\eta^2\left\{(2\alpha+\gamma)\Omega^2 + 2\alpha\gamma\eta^2\right\} - 4\alpha^2\gamma\Theta_b\eta^2k^2$$
$$-\left\{\Theta_n\Omega^4 - 2\alpha(\gamma\Theta_b - \Theta_n)k^2\Omega^2 - 4\alpha^2\gamma\Theta_b\eta^2k^2\right\}$$
$$-\frac{d\ln W}{d\zeta}\gamma\Omega^2(\Omega^2+2\alpha\eta^2) - \Theta_n\gamma\Omega^2(\Omega^2+2\alpha\eta^2)$$
$$-2\alpha\left[\Theta_b\Omega^4 + \left\{(\gamma\Theta_b - \Theta_n)\xi^2 + (2\alpha+\gamma)\Theta_b\eta^2\right\}\Omega^2\right]$$
$$-2\alpha\left(\frac{d\ln W}{d\zeta} + 2\Theta_b\right)(\Omega^2+2\alpha\eta^2)(\Omega^2+\gamma\eta^2)$$
$$+\left\{(1+\alpha)\Theta_n - \frac{d\alpha}{d\zeta}\right\}\Omega^2(\Omega^2+2\alpha\eta^2)$$

$$A_0 \equiv -\frac{d\Theta_n}{d\zeta}\Omega^4 + 2\left(\gamma\frac{d\alpha\Theta_b}{d\zeta} - \frac{d\alpha\Theta_n}{d\zeta}\right)k^2\Omega^2$$
$$-4\gamma\eta^2k^2\frac{d\alpha^2\Theta_b}{d\zeta} - W(\Omega^2+2\alpha\eta^2)$$
$$+(\frac{d\ln W}{d\zeta} + \Theta_n)\{\Theta_n\Omega^4 - 2\alpha(\gamma\Theta_b - \Theta_n)k^2\Omega^2$$
$$-4\alpha^2\gamma\Theta_b\eta^2k^2\}$$
$$+4\alpha\Theta_b[\Theta_b\Omega^4 + \{(\gamma\Theta_b - \Theta_n)\xi^2 + (2\alpha+\gamma)\Theta_b\eta^2\}\Omega^2$$
$$+2\alpha\gamma\Theta_b\eta^2k^2]$$
$$-2\alpha[\frac{d\Theta_b}{d\zeta}\Omega^4 + \{(\gamma\frac{d\Theta_b}{d\zeta} - \frac{d\Theta_n}{d\zeta})\xi^2$$
$$+(2\frac{d\alpha\Theta_b}{d\zeta} + \gamma\frac{d\Theta_b}{d\zeta})\eta^2\}\Omega^2 + 2\gamma\eta^2k^2\frac{d\alpha\Theta_b}{d\zeta}]$$
$$+2\alpha\frac{d\ln W}{d\zeta}[\Theta_b\Omega^4 + \{(\gamma\Theta_b - \Theta_n)\xi^2$$

$$+(2\alpha+\gamma)\Theta_b\eta^2\}\Omega^2+2\alpha\gamma\Theta_b\eta^2k^2]$$

$$+\{\frac{d\alpha}{d\zeta}-(1+\alpha)\Theta_n\}[\Theta_n\Omega^4-\{(1-2\alpha-\gamma)\Theta_n$$

$$+2\alpha\Theta_b\}k^2\Omega^2-2\alpha\{(1-\gamma)\Theta_n+2\alpha\Theta_b\}\eta^2k^2]$$

$$B_1\equiv-\Omega^3(\Omega^2+2\alpha\eta^2)$$

$$B_0\equiv2\gamma\eta^2k^2\frac{d\alpha}{d\zeta}\Omega-\Theta_n\gamma k^2\Omega(\Omega^2+2\alpha\eta^2)-4\alpha\Theta_b\xi^2\Omega^3$$

$$-2\alpha\frac{d\ln W}{d\zeta}\xi^2\Omega^3-\{\frac{d\alpha}{d\zeta}-(1+\alpha)\Theta_n\}k^2\Omega(\Omega^2+2\alpha\eta^2)$$

$$-\frac{d\ln W}{d\zeta}\gamma k^2\Omega(\Omega^2+2\alpha\eta^2)$$

$$C_2\equiv W\Omega$$

$$C_0\equiv-k^2\Omega[\Omega^4-\{S_v(\zeta)-(2\alpha+\gamma)k^2\}\Omega^2$$

$$+2\alpha\{\gamma k^2-S_v(\zeta)\}\eta^2]$$

$$D_1\equiv S_v(\zeta)\Omega^2(\Omega^2+2\alpha\eta^2)$$

$$D_0\equiv-S_v(\zeta)[\Theta_n\Omega^4-\{(1-2\alpha-\gamma)\Theta_n+2\alpha\Theta_b\}k^2\Omega^2$$

$$-2\alpha\{(1-\gamma)\Theta_n+2\alpha\Theta_b\}\eta^2k^2]$$

Here all symbols have the same meaning as in section 3.

REFERENCES

Alfaro, E. J., Cabrera-Cano, J., & Delgado, A. J. 1992, ApJ, 399, 576

Bienayme, O., Robin, A. C., & Creze, M. 1987, A&A, 180, 94

Boulares, A., & Cox, D. P. 1990, ApJ, 365, 544

Dickey, J. M., Murry H. M., & Helou, G. 1990, ApJ, 352, 522

Elmegreen, B. G. 1992, in The Galactic Interstellar Medium, ed D. Pfenniger & P. Bartholdi (Saas-Fee Course; Berlin: Springer), 157

Elmegreen, B. G. 1993, in Star Formation, Galaxies, and the Interstellar Medium, ed. J. Franco, F. Ferrini, & G. Tenorio-Tagle (Cambridge: Cambridge Univ. Press), 335

Elmegreen, B. G., & Elmegreen, D. M. 1987, ApJ, 320, 182

Franco, J., Kim. J., Alfaro, E., & Hong, S. S. 2002, ApJ, 570, 647 (Paper III)

Gum, C. S., Kerr, F. J., & Westerhout, G. 1960, MNRAS, 121, 132

Heiles, C. 1995, in The Physics of the Interstellar Medium and Intergalactic Medium, ed. A. Ferrara, C. F. MaKee, C. Heiles, & P. R. Shapiro (San Francisco: ASP), 507

Kim, J., & Hong, S. S. 1998, ApJ, 507, 254

Kim, J., Franco, J., Hong, S. S., Santillan, A., & Martos, M. A. 2000, ApJ, 531, 873 (Paper I)

Kim, J., Ryu, D., Jones, T. W., & Hong, S. S. 1999, ApJ, 514, 506

Lee, S. M., & Hong, S. S. 2004, ApJ, in preparation

Lee, S. M. 2002, PhD Thesis, Seoul National University

Lee, S. M., & Hong, S. S. 1999, in Proceeding of the 4th East Asian Meeting on Astronomy, 293

Liszt, H. S. 1985, in IAU Symp. 106, The Milky Way Galaxy, ed. H. van Woerden, R. J. Allen, & W. B. Burton (Dordrecht: Reidel), 283

Martos, M. A. 1993, Ph. D. thesis, Univ. Wisconsin, Madison

Martos, M. A., & Cox, D. P. 1998, ApJ, 509, 703

Martos, M. A., Allen, C., Franco, J., & Kurtz, S. 1999, ApJ, 526, L89

Parker, E. N. 1966, ApJ, 145, 811

Santillan, A., Kim, J., Franco, J., Martos, M., Hong, S. S., & Ryu, D. 2000, ApJ, 545, 353 (Paper II)

Tomisaka, K., & Ikeuchi, S. 1983, PASJ, 35, 187